Journal of Applied Electrochemistry **31**: 1203–1212, 2001.

Electroplating and electroless plating of Ni through/onto a porous polymer in a flow cell

I.J. BROWN[1] and S. SOTIROPOULOS[2]*
[1]*School of Chemical, Environmental and Mining Engineering, Nottingham University, University Park, Nottingham NG7 2RD, Great Britain*
[2]*Chemistry Department, Aristotle University of Thessaloniki, Thessaloniki 54006, Greece*
*(*author for correspondence)*

Received 10 January 2001; accepted in revised form 10 July 2001

Key words: hydrogen evolving cathodes, metal foams, porous Ni coatings, porous polymers

Abstract

Porous Ni coatings on electrodes were produced by electroplating through the cells and pores of a generic 'high internal phase emulsion polymer' (PHIPE), a styrene-ethylhexylacrylate-divinylbenzene copolymer, and subsequent thermal decomposition of the polymer template. Electroplating was carried out from flowing solutions through a polymer block fitted in the interelectrode gap of a flow-by cell. The mass transfer conditions and the flow regime in the cell were also characterized. The structure of the porous electrodeposits thus produced was determined by the distortion of the electric field through the cells and pores of the insulating polymer and depends on the current density and the thickness of the polymer layer. Porous deposits plated at 5 mA cm^{-2} showed high utilization of electroactive surface area when used as hydrogen evolving cathodes from alkaline solutions. Finally, Ni/PHIPE composite foams were prepared by Ni electroless plating through the polymer pores and their electrochemical surface area was evaluated.

1. Introduction

The electrochemical or chemical (electroless) deposition of metals through/onto porous templates or supports finds a number of applications in catalysis (and electrocatalysis), electrochemical sensors, the production of composite materials and in microfabrication. In the fields of catalysis and separation processes examples include the use of metallized porous membranes as catalytic reactors [1] and in filtration processes [2, 3]. Electrochemical or electroless metal deposition is one of the techniques employed in the production of high surface area electrodes used in fuel cells and batteries whereby the electrocatalyst (e.g., Pt, Ni etc.) is deposited onto a conducting porous substrate (e.g., foam [4] or reticulated [5, 6] electrodes). Microfabrication applications include plating through patterned polymers produced by lithographic techniques [7], or through microporous and nanoporous solid templates such as polymeric membranes, anodized alumina or porous mica [8–10]. The latter was initially introduced for the production of microelectrode arrays [8] and subsequently used for the preparation of nanowires of unique catalytic, optical and magnetic properties, following the decomposition of the template material [9, 10].

High surface area Ni electrodes are used as hydrogen evolving cathodes in water electrolysis [11, 12] and the chlor-alkali industry [13], NiO(OH) cathodes in nickel–cadmium and nickel–hydrogen batteries [14] and as anodes in alkaline or molten carbonate fuel cells [15]. They are also found in the electrochemical hydrogenation of organics [16] and as three-dimensional foam electrodes both for the electrolytic recovery of metals [17] and in electroorganic synthesis [18]. A large variety of preparation methods for high surface area Ni electrodes exist. The ceramic foil-casting technology [13] produces microporous sintered Ni coatings (pore diameter in the μm range) and a review of the methods for nanoporous Raney–Ni coatings production is given by Rausch and Wendt [19].

We have recently prepared small Ni/polymer composites by electroless deposition and electroplating from stationary solutions onto/through the pores of PHIPE, a microporous generic polymer [20–24] (pore size in the μm range; also referred to as macroporous according to the IUPAC terminology). PHIPEs are copolymers formed by emulsion polymerization of 'high internal phase water-in-oil emulsions' (HIPEs), where the volume of the aqueous dispersed phase is greater than about 75%, and the subsequent polymerization (at 60 °C) of the oil phase which contains the monomer (typically styrene and other monomers such as alkylacrylates) and the cross-linker (divinyl-benzene) [25]. The resulting polymer matrix shows an extremely high

voidage (up to 97%) due to the evaporation of the water droplets, which were present in the precursor emulsion. According to the most recent modification of the proposed preparation technique for microporous Ni electrode coatings [21, 22], the electrode substrates are immersed in the precursor emulsion and, upon polymerization, entrapped within the polymer matrix. Subsequently, the metal is electroplated through the pores of the PHIPE coating onto the substrate and finally, the polymer is thermally decomposed.

In this work, the first steps towards a potential scaling-up of the above Ni electroplating process are attempted using a bench-scale parallel-plate flow-by electrochemical cell, modified to accommodate a block of PHIPE tightly fitted in the interelectrode gap. Increasing mass transfer conditions by flowing the electroplating solution (through the polymer) is expected to improve the uniformity and adherence of the porous electrode coatings, by extending the regime of electron transfer control (which is known to result in even and adherent deposits) [26–28]. This is especially important in electroplating through porous templates which is inherently associated with nonuniform current distribution and hence, a tendency for uneven deposits [29]. The porous Ni coatings are evaluated as hydrogen evolution catalysts and compared to sintered Ni electrodes while the mass transfer regime within the flow-cell in the presence and absence of PHIPE is also studied.

We also present results of Ni electroless deposition on PHIPE, whereby the plating solution is pumped through the polymer samples. This should prevent hydrogen (a byproduct of Ni electroless deposition) entrapment in the polymer cells and pore blanketing, thus increasing the Ni penetration depth beyond the outer sample surface [20]. The resulting Ni/PHIPE foam composites are characterized with respect to their electroactive surface area based on Ni surface electrochemistry [30, 31].

2. Experimental details

2.1. *PHIPE polymer preparation and decomposition*

Polymer of 80% voidage was produced using 80% v/v aqueous phase in the precursor water-in-oil emulsion. The composition of the oil phase was (by volume): 15% styrene (Aldrich, 99%), 62% 2-ethyl-hexyl-acrylate (Aldrich), 8% divinylbenzene (Aldrich, 80%) and 15% sorbitan monooeleate (Aldrich, 95%). The aqueous phase was distilled water and 1% w/w potassium persulphate (Aldrich, 99% +) that acted as the polymerization initiator. Typically, 500 ml batches of precursor emulsion were produced by careful mixing of the two phases in a stainless steel, watertight vessel, equipped with a Janke and Kunkel (IKA Labortechnik) model RW 20DZM two-blade mixer according to a procedure described previously [20, 21]. A portion of the emulsion was then poured into an appropriate polypropylene mould (a shallow tray of 105 mm × 105 mm area and 18 mm depth) and covered tightly with parafilm to minimize water evaporation during polymerization, which was performed for 6 h in an oven heated at 60 °C. After polymerization the samples remained uncovered for another 24 h in the oven for residual water to be driven off. In this way, polymer blocks of 100 mm × 100 mm × 15 mm approximate dimensions (PHIPE shrinks upon formation) were produced to fit in the rectangular central part of the flow cell frame (see below).

The structure of PHIPE thus produced is shown in the SEM micrograph of Figure 1 (a Hitachi S-570 SEM was used). It is characterized by numerous cells (10–30 μm diameter) corresponding to emulsion water droplets, interconnected by smaller pores (0.1 to 1 μm diameter) corresponding to droplet contact areas.

Thermal decomposition of the polymeric matrix of the Ni/PHPIPE composites after electroplating was carried out under an air atmosphere in a preheated furnace at 450–500 °C, for 1 h. The resulting material was treated for 30 min in a boiling 40% v/v solution of hydrogen peroxide to oxidize any residual organics. SEM and EDAX analysis confirmed complete polymer burnout at the end of this procedure [20]. Prior to electrochemical experiments, samples were immersed in 1:1 30% HCl:water mixture for 30 s to dissolve any surface Ni oxides.

2.2. *Electroplating flow cell and procedure*

The parallel plate flow cell shown in Figure 2(A) was based on a plate-and-frame assembly. The two end plates held the two stainless steel current collectors and the entrance and exit ports for the electrolyte. The frame had a cross-sectional area of 15 cm^2 (1.5 cm × 10 cm) for flow, with a projected area of 100 cm^2, while the gaskets were made from PTFE.

Electrical contacts to the stainless steel current collectors were made by stainless steel threaded bars. The working electrodes were 5 cm × 5 cm Ni plates (99.0%, 0.25 mm thick, Goodfellow Ltd) or Ni meshes (99.0%, 26 × 26 wires per inch, 0.25 mm thick, Goodfellow Ltd).

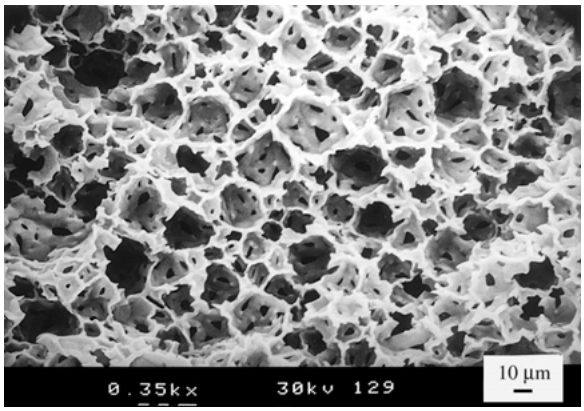

Fig. 1. SEM micrograph of PHIPE polymer.

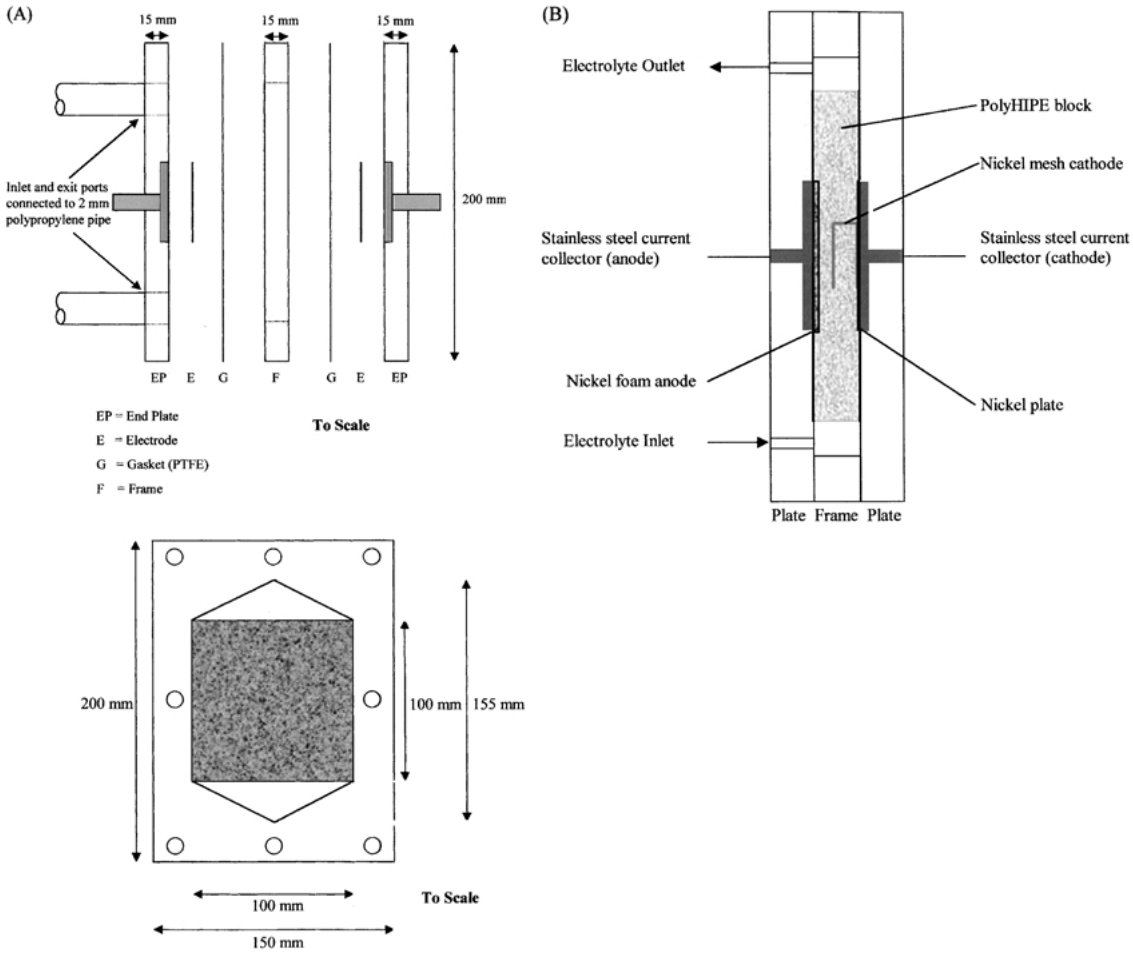

Fig. 2. (A) Schematic diagram of parallel plate flow-by electroplating cell (side view) and frame (front view). (B) Schematic diagram of a modification of the cell of (A) above, with a Ni mesh pocket-shaped cathode embedded in the polymer interelectrode block.

The counter electrode was a 1.6 mm thick, 5 cm × 5 cm Ni foam (96.5% porosity, 43 pores cm^{-1}, Goodfellow Ltd). Both electrodes were attached to the current collector using carbon cement (WPI) and a 10 cm × 10 cm, 1.5 cm thick PHIPE block was fitted in the interelectrode gap. In a modified set of experiments the polymer had a Ni mesh pocket electrode embedded to it (by immersion in the precursor emulsion), with one side of the pocket protruding from the block and in contact with the Ni plate (Figure 2(B)). The side of the pocket closest to the counter electrode was approximately at a distance of 0.5 cm from it. A 1 mm thick Pt wire (99%, Goodfellow Ltd) inserted through the gasket and lying 2 mm away from the working electrode served as a reference electrode.

The hydraulic flow circuit consisted of a Totton NEMP 40/11 polypropylene pump, a polypropylene rotameter, and a thermostated (25 °C) 1.6 litre glass/polypropylene reservoir. The flow rates studied were in the 1–15 cm s^{-1} linear velocity, v, range. Pressure tapings were placed alongside the inlet and outlet ports to the flow cell and connected to an air over water-inverted manometer to monitor pressure drop through the cell. A standard nickel sulphamate bath [26, 27] was used as the electroplating solution at 60 °C: 600 g l^{-1} nickel sulphamate (Aldrich, 98%), 10 g l^{-1} nickel chloride (Aldrich) and 40 g l^{-1} boric acid (Aldrich, 99.5 + %). Constant current electroplating was carried out with an Autolab 30 potentiostat/galvanostat (Eco Chemie, Windsor Scientific Ltd) or a TCX1820P programmable d.c. power supply (20 A, 18 V).

2.3. *Electroless plating flow cell and procedure*

A small flow cell consisting of a 1.4 cm internal diameter glass tube (QVC) connected to glass tubing with PTFE gaskets was used for electroless plating. The inlet and outlet were further connected to Fisher Silicon Tubing suitable for use with a Watson Marlow peristaltic pump. PHIPE tubular samples were held in the tube cell by a PTFE gasket with a 1.2 cm diameter. The glass part of the assembly was immersed in a thermostated bath. PHIPE was sensitized with a $SnCl_2$ + $PdCl_2$ solution and a standard nickel chloride-hypophosphite bath was used at 93 °C for the Ni electroless plating step [26].

2.4. *Electrode characterization*

All potentiodynamic, potentiostatic and galvanostatic experiments were carried out with an Autolab 30

potentiostat/galvanostat (Eco Chemie, Windsor Scientific Ltd), with current-interrupt IR compensation. For flow cell characterization experiments potassium ferricyanide(III) trihydrate (99%+, Aldrich) and Potassium Ferrocyanide(II) trihydrate (99%, Aldrich) solutions in 1 M degassed sodium hydroxide (99.99%, Aldrich) were used. The Ni working electrode was cathodized at 10 mA cm^{-2} in the hydroxide solution prior to these experiments.

Ni surface electrochemistry and hydrogen evolution were studied in degassed 0.5 M NaOH solutions at 25 °C. A three-electrode cell with a Pt coil counter electrode (BAS Technicol Ltd) and a saturated calomel electrode (SCE, EG&G) equipped with a salt bridge ending to a Vycor® tip (EG&G), were used.

3. Results and discussion

3.1. *Flow-cell characterization with and without PHIPE in the interelectrode gap*

Figure 3 shows slow potential sweep voltammograms for the reduction of ferricyanide from a 5 mM ferricyanide + 20 mM ferrocyanide excess solution in 1 M NaOH, at 1 mV s^{-1} sweep rate, without or with (Inset) PHIPE in the interelectrode gap. The upper limit for experiments with PHIPE is due to the large pressures drops encountered and the limitations of the pumping system. For an accurate determination of the mass transfer limiting current we employed the method introduced by Cowan and Brown [32] and recently modified by Ponce-de-Leon and Field [33], whereby I/E (current against electrode potential) curves are replotted as E/I against $1/I$ curves and the limiting current is obtained from the point where their slope changes sign. The limiting current densities, j_L, thus obtained where used in the equation

$$j_L = nFk_Lc \quad (1)$$

to obtain the mass transfer coefficient k_L (c is the concentration of the electroactive species and n the number of electrons involved in the electrode reaction). Figure 4(A) shows the variation of log k_L with log v in the absence or presence of PHIPE (the area occupied by the polymer and the foam anode was taken into account, when needed, in calculations of v). The slopes obtained where 0.62 and 0.53, respectively (although the latter should be treated cautiously due to the limited range in PHIPE experiments), and the presence of PHIPE increases the mass transfer to the electrode by a moderate factor of about 1.7. This enhancement lies in the lower range of that of a number of bulk turbulence promoters studied by Brown et al. [34]. The small increase in k_L introduced by PHIPE may be due to a possible underestimation since parts of the electrode surface should be blocked by the polymer and/or the special features of flow through the porous polymer and past the polymer/electrode interface. The very high surface area of the material should have a calming effect on the flow and suppress turbulence. The Inset to Figure 4(A) shows the double logarithmic plots of the Sherwood (Sh) against Reynolds (Re) number. The values of $D = 6.5 \times 10^{-6}$ cm^2 s^{-1} (found from cyclic voltammetric experiments in 1 M NaOH using a Ni disc

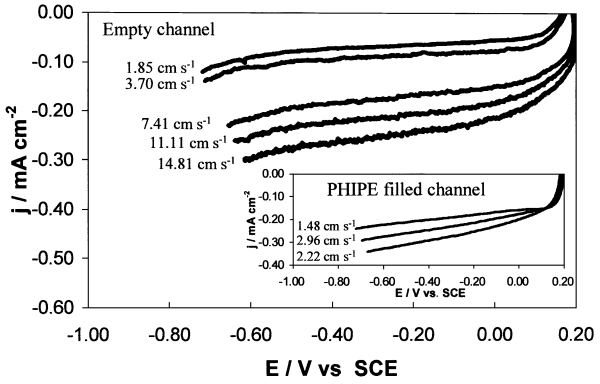

Fig. 3. Current–potential curves for ferricyanide reduction from a 5 mM potassium ferricyanide solution in 20 mM potassium ferrocyanide and 1 M NaOH, recorded in the empty channel flow cell of 2(A) on a Ni plate electrode at a 1 mV s^{-1} potential sweep rate, for a number of linear flow velocity values. Inset: same as above but in the presence of a PHIPE polymer block in the interelectrode gap.

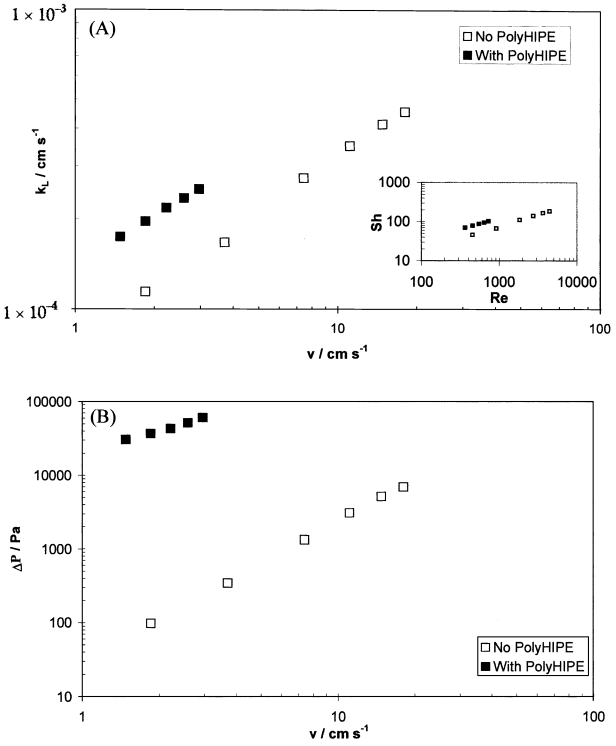

Fig. 4. (A) Log–log plot of mass transfer coefficient for ferricyanide reduction in the flow cell of 2(A) above against the linear flow velocity, in the absence and presence of PHIPE. Inset, double logarithmic plot of Sherwood number (Sh) against the Reynolds number (Re). (B) Log–log logarithmic plot of the pressure drop between the inlet and outlet of the cell against linear flow velocity, in the absence and presence of PHIPE for the flow cell of 2(A) above.

electrode) and $v = 1.0556 \times 10^{-6}$ m^2 s^{-1} were used for the calculation of the *Re*, *Sh* and *Sc* (Schmidt) numbers, and the hydraulic diameter of the empty rectangular channel [35], d_e, for that of *Re*. The dimensionless group correlations from the inset of Figure 4(A) without and with PHIPE are, respectively:

$$Sh = Re^{0.62} Sc^{0.33} \quad (2)$$

and

$$Sh = 3.09\, Re^{0.53} Sc^{0.33} \quad (3)$$

The value of 0.62 for the slope of the log *Sh* against log *Re* curve for the empty channel is very close to the value of 0.66 found for fully developed turbulent flow with short ($L/d_e < 10$) electrodes [36]. The reason why the turbulent flow regime extends to *Re* values below 2300 (where laminar flow is expected [37]) could be due to the 90° change in flow direction at the cell entry and exit in connection with the short (~2 cm) entry and exit lengths, the fact that the working electrode plate was not recessed in the cell walls and the use of a thin three-dimensional Ni foam anode. Values higher than 0.33 are common for $Re < 1000$ (e.g., 0.47 in [38], 0.70 in [34]), and these are highly dependent on cell design and components. The slope of 0.53 obtained in the presence of PHIPE (similar to [34] where the presence of the promoter led to a lower slope and was attributed to partial flow laminization) indicates that the polymer block insert does not increase the degree of turbulence, due to its very high surface area. It should be noted that, although in similar electrochemical studies of flow through porous Ni foam electrodes the Reynolds number in dimensionless group correlations was based on the hydraulic diameter of the empty channel [18, 39], an accurate description of the flow through a porous medium would require the use of an interstitial Reynolds number Re_i defined as [40, 41]:

$$Re_i = \frac{v d_{e,i}}{\nu} \quad (4)$$

where $d_{e,i}$ is the equivalent diameter of the pore space. In the case of reticulated Ni foams with a regular open structure the mean pore diameter could be used [40] but in the case of the less regular PHIPE structure with a distribution of cell and pore size (Figure 1) we calculated an equivalent diameter based on [41]:

$$d_{e,i} = \frac{\varepsilon}{S(1-\varepsilon)} \quad (5)$$

where ε is the porosity of the medium (0.8 for PHIPE) and *S* the specific surface area per unit volume (we used the 5 m^2 g^{-1} found by BET measurements [20, 21] to calculate this). We thus estimated an effective diameter of 5.3 μm and Re_i numbers in the 0.07–0.15 range; these very low numbers correspond to the Darcy or creeping flow regime through porous media [38, 40]. However, the flow conditions at the electrode–fractured PHIPE interface are likely to differ significantly from that through the bulk polymer and some limited turbulence is expected, giving rise to the moderate enhancement in k_L, shown in Figure 4(A).

Finally, Figure 4(B), which presents the double logarithmic plot of pressure drop ΔP between the inlet and outlet of the cell in the absence and presence of PHIPE as a function of *v*, shows that the incorporation of the polymer block introduces an almost four hundredfold increase in pressure drop, further indicating that the material is unsuitable as a potential turbulence promoter and highlighting limitations in using it in a thinner interelectrode gap.

3.2. *Ni electroplating through PHIPE and Ni coating evaluation as hydrogen cathodes*

Figure 5(A) is the SEM micrograph of the Ni electrodeposit on a Ni plate cathode by electroplating through PHIPE at 5 mA cm^{-2} and a solution linear velocity of 1.5 cm s^{-1}, after polymer decomposition. An adherent nodular deposit having a uniform thickness of 410 μm was produced over the entire surface of the 5 cm × 5 cm Ni plate. A current efficiency of about 97% was found and a porosity of 40% could be estimated. At higher

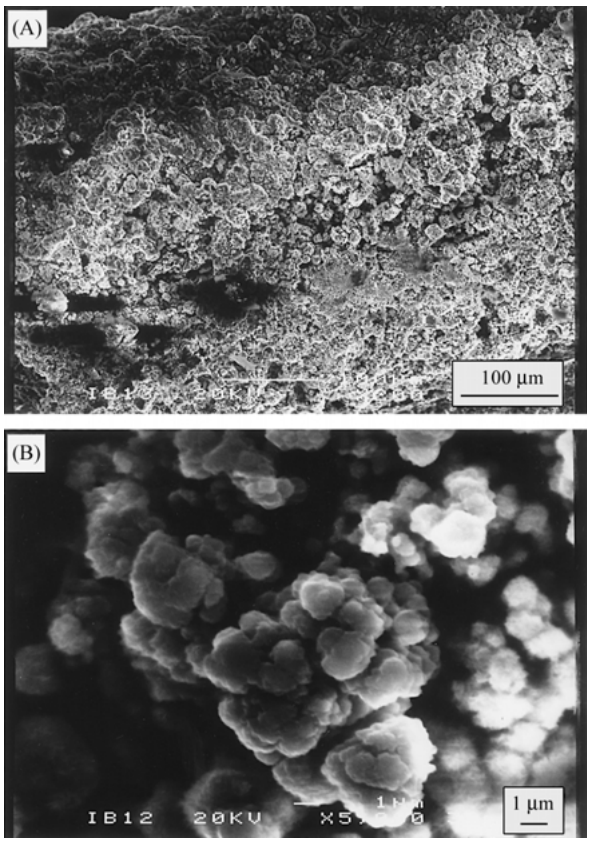

Fig. 5. SEM micrographs of a Ni electrodeposit produced at 5 mA cm^{-2} and at 1.5 cm s^{-1} in the cell of Figure 2(A), at different magnifications (A) and (B).

magnifications, see Figure 5(B), the deposit is shown to be made up of near spherical agglomerates 1–10 μm in diameter (with a wide size distribution) and fewer voids of similar dimensions. Although there is no straightforward host-guest relationship between the polymer matrix and the metal deposit, we believe that the structure of the Ni deposit is due to the distortion of the electric field in the presence of the insulating PHIPE porous shield [42]. For an electrodeposit growing through a tortuous cell-and-pore path the local current density around the cell pores will be significantly higher than the average, resulting in a nodular [35] or unoriented dispersion type [28] deposits, even in the absence of inhibitors. During the thickening process, once an entire cell is filled (or partially filled) with Ni, deposition will preferentially continue through a neighbouring cell closer to the anode rather than through a cell at the same plane, due to ohmic losses through the porous nonconducting medium. This effect will lead to either partially filled or completely void polymer cells in accordance with Figures 5(A) and 5(B) above. Flow increases the mass transfer coefficient and replenishes the Ni ion concentration in the polymer cells at the electrode surface, thus extending the kinetic control regime and imposing limitations on the deposit irregularity. The latter is essential if porous deposits are to be obtained throughout the entire surface of large electrodes, where the high electroplating currents result in higher ohmic losses, which in turn may accentuate uneven growth. Therefore attempts to electroplate large substrates from stationary solutions resulted in uneven nonadherent deposits. The same effect was observed when trying to electroplate at higher current densities, even from flowing solutions. Figure 6 presents micrographs of different locations of a Ni/PHIPE composite (before polymer decomposition) produced by electroplating at 50 mA cm^{-2} at a flow rate of 1.5 cm s^{-1}. The micrograph of Figure 6(A) shows the Ni layer produced at the PHIPE surface in contact with the metal cathode and a Ni deposit organised in aggregates occupying the cells of the PHIPE surface layer is observed. Figures 6(B) and 6(C) show two different locations in the bulk of the composite highlighting its uneven lateral growth and structure. In Figure 6(B) big isolated spherical Ni deposits are seen, occupying only a small number of cells, on a location close to the electrode surface, most likely corresponding to a low local current density due to high ohmic losses. In Figure 6(C), much smaller aggregates can be seen closer to the anode. These are interconnected by needless of submicrometric length, a deposit morphology which many result from high local current densities [21].

To minimize the effect of substantial IR drop on deposit uniformity at relatively high current densities, electroplating of thinner layers was carried out using the cell of Figure 2(B), where the interelectrode gap, 0.5 cm,

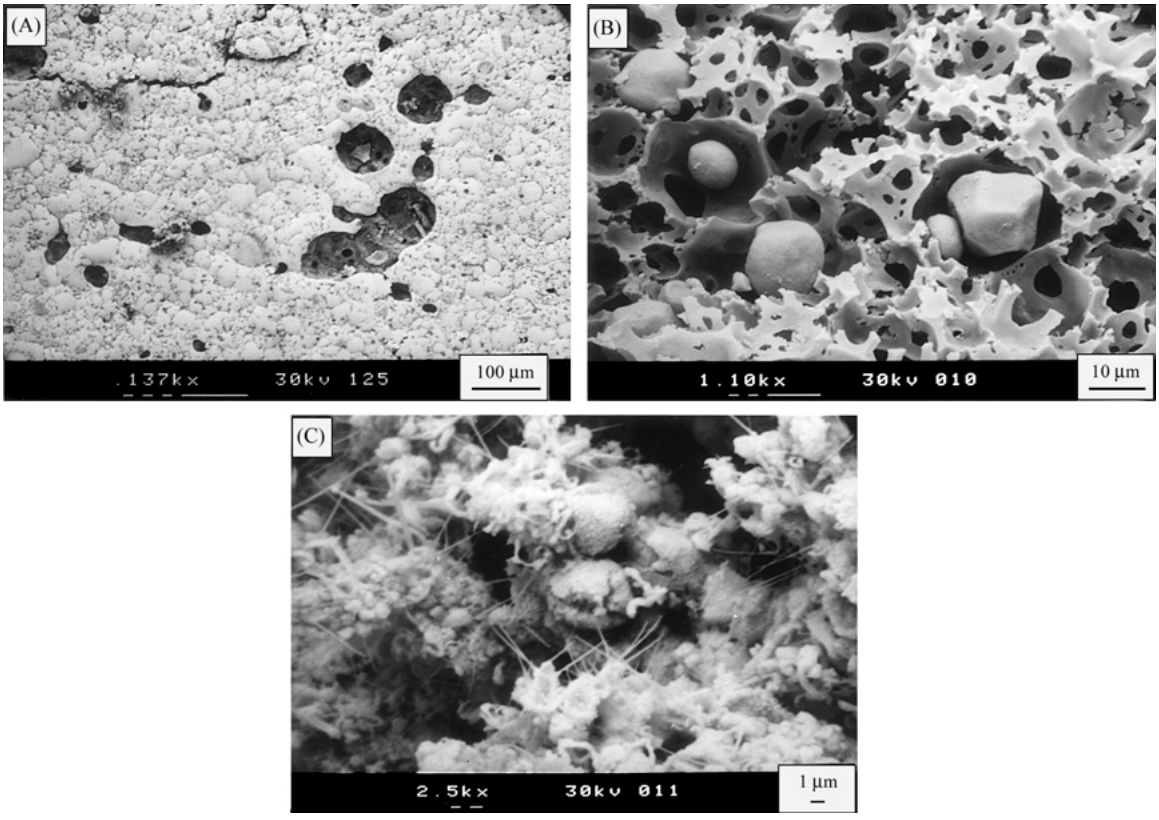

Fig. 6. SEM micrographs of a Ni/PHIPE composite produced at 50 mA cm^{-2} and at 1.5 cm s^{-1} in the cell of 2(A): (A) surface in contact with the electrode–polymer interface; (B) location of limited electrodeposition in the polymer body; (C) location of thick electrodeposit in the polymer body close to the anode.

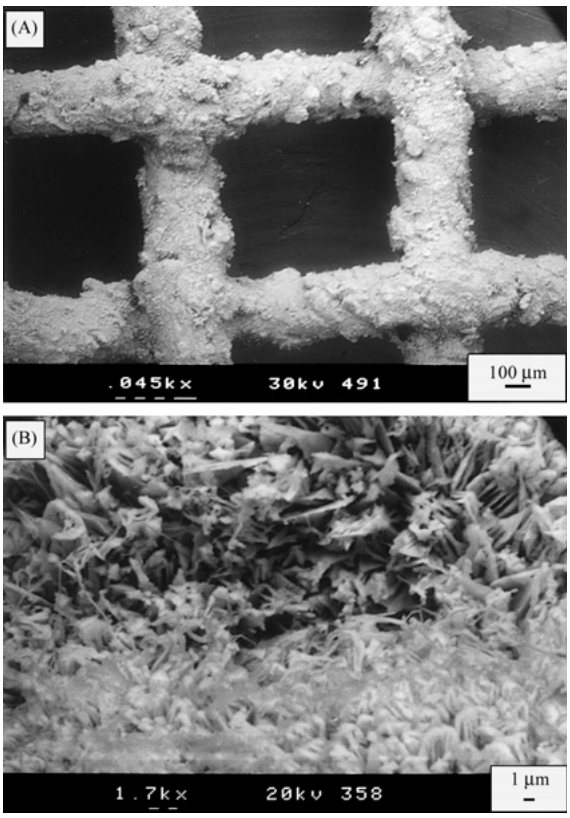

Fig. 7. SEM micrographs of a 0.25 mm diameter wire Ni mesh electroplated with Ni at 50 mA cm^{-2} and at 1.5 cm s^{-1} in the cell of 2(B): (A) general view; (B) deposit detail.

was also approximately one-third of that previously used. Figure 7(A) shows the micrograph of a Ni mesh electrode fully covered with an adherent deposit (average thickness about 75 μm) undulated with small clusters, after electroplating at 50 mA cm^{-2} at a 1.5 cm s^{-1} flow rate. A detail of the deposit (Figure 7(B)) reveals that it is made of flakes of a few μm dimensions.

The Ni coatings thus produced were evaluated as hydrogen evolving cathodes in 0.5 M NaOH solutions and compared with typical sintered electrodes [19] and similar deposits obtained through PHIPE from stationary solutions but onto small substrates [22]. A potential sequence was applied to the electrodes to ensure surface reproducibility [22, 31, 43] before the potential was kept constant for 5 min to obtain near steady-state current–potential data. Table 1 presents the thickness, porosity, roughness factor and specific area of a smooth Ni disc, nickel wires, plates and meshes electroplated through PHIPE using flowing and stationary [22] electroplating solutions and for a sintered nickel coating, consisting of sintered Ni particles of 2–3 μm diameter [19]. The roughness factor and specific area were calculated using the electroactive surface area, measured from the charge associated with the formation/stripping of a $Ni(OH)_2$ monolayer in the potential region prior to hydrogen evolution, as found by cyclic voltammetry [30, 31]. Figure 8(A) presents the log j against E curves (j given as current per substrate geometric area) and for comparison, data for a sintered Ni coating as described in Table 1. Similar or improved current densities can be obtained at deposits produced through PHIPE. A convenient parameter used to compare porous coatings is the electrode volume, V_e. Figure 8(B) presents the log j against E curves (j given as current per coating volume) for the Ni coatings described in Table 1. The Ni coatings produced by electroplating through the PHIPE template have a similar performance to typical sintered Ni coatings, even though the electroactive surface area per unit coating volume of the former are an order of magnitude lower than that for sintered Ni [19]. The degree of electroactive area utilization is shown in Figure 8(C) where log j against E curves are presented with j given as current per electroactive surface area, (esa) using the areas detailed in Table 1. For the 5 and 10 mA cm^{-2} produced coatings almost the entire electroactive surface area is utilized for the hydrogen evolution reaction (as indicated by the near coincidence of the data with those for smooth Ni). In contrast, at an overpotential value of −130 mV (i.e., at −1.2 V vs SCE,

Table 1. Thickness, porosity, roughness factor and specific area of nickel-coated electrodes produced by electroplating through PHIPE sandwiched in the flow cell
Data for a polished nickel disc, a Ni wire electroplated through PHIPE from a stationary electrolyte and a sintered nickel electrode are included for comparison

	Electroplating current density/mA cm^{-2}	Electrolyte velocity/cm s^{-1}	Thickness* /μm	Porosity†	Roughness Factor, r‡/cm^2 cm^{-2}	Specific Area, A_e§/m^2 m^{-3}
Ni plate in PHIPE	5	1.5	410	0.40	20	43,000
Ni mesh in PHIPE	50	1.5	75	0.88	6	45,000
Polished Ni disc	n/a	n/a	n/a	n/a	1.3	n/a
Ni wire in PHIPE [22]	10	0.0	700	0.54	86	70,000
Sintered Ni [19]	n/a	n/a	350	0.60	270	770,000

* The thickness of the coatings was measured using a micrometer and SEM micrographs.
† The porosity of the coatings was calculated from the volume (calculated from the thickness) and mass of the nickel coating (measured by weighing the substrates before and after electroplating).
‡ The roughness factor is the ratio of the electrochemical surface area (measured from the charge associated with the formation/stripping of a monolayer of $Ni(OH)_2$) with geometric substrate area.
§ The specific area is the ratio of the electrochemical surface area with the volume of the nickel coating.

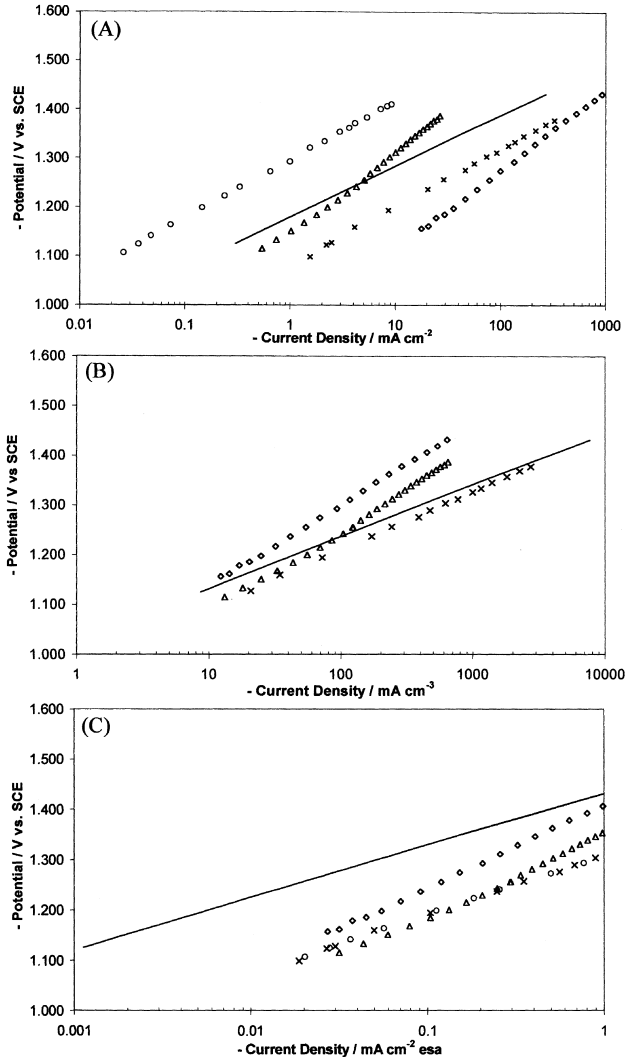

Fig. 8. (A) Semilogarithmic current (per substrate geometric area) against potential curves for hydrogen evolution from 0.5 M NaOH solutions at Ni electrodes: 5 mA cm^{-2} plated plate (△) and 50 mA cm^{-2} plated mesh (◇) both electroplated with an electrolyte velocity of 1.5 cm s^{-1} in the flow cell; smooth Ni (○); 10 mA cm^{-2} plated wire in stationary electrolyte (×) [22] and sintered Ni [19] (–). (B) Semilogarithmic current (per coating volume) against potential curves for hydrogen evolution from 0.5 M NaOH solutions at Ni electrodes: 5 mA cm^{-2} plated plate (△) and 50 mA cm^{-2} plated mesh (◇) both electroplated with an electrolyte velocity of 1.5 cm s^{-1} in the flow cell; 10 mA cm^{-2} plated wire in stationary electrolyte (×) [22] and sintered Ni [19] (–). (C) Semilogarithmic current (per electroactive surface area) against potential curves for hydrogen evolution from 0.5 M NaOH solutions at Ni electrodes: 5 mA cm^{-2} plated plate (△) and 50 mA cm^{-2} plated mesh (◇) both electroplated with an electrolyte velocity of 1.5 cm s^{-1} in the flow cell; smooth Ni (○); 10 mA cm^{-2} plated wire in stationary electrolyte (×) [22] and sintered Ni [19] (–).

since the reversible potential in our system is −1.060 V vs SCE) the current at sintered Ni electrodes is only 5% of that at smooth or 5 and 10 mA cm^{-2}-produced samples, and that at the 50 mA cm^{-2}-produced sample is 50%. The utilization drops in the case of the sintered Ni coating and the Ni-coated mesh, probably due to increased hydrogen entrapment-blanketing within the sintered Ni [19] and the densely packed flakes of the Ni-coated mesh. The large voids between the Ni aggregates

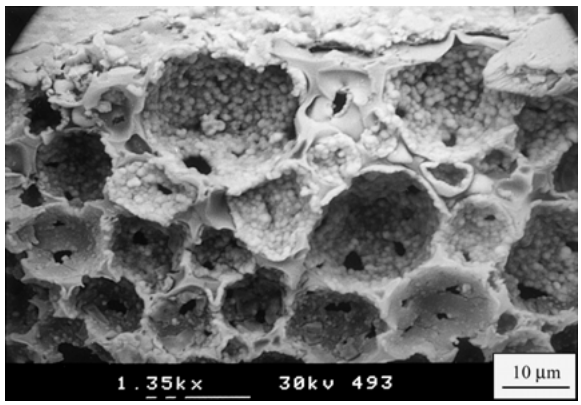

Fig. 9. SEM micrograph of a PHIPE sample coated by Ni electroless plating with a solution pumped through the polymer.

of the other coatings (Figure 5(B)) allow hydrogen gas to disengage easily, leading to high utilization of the surface area.

3.3. *Ni electroless plating onto PHIPE*

Figure 9 presents the SEM micrograph of a cross section of a PHIPE sample treated with a Ni electroless plating solution pumped at a volumetric flow rate of 14 l h^{-1} through the polymer for 45 min. The internal surface is completely covered with a Ni deposit made of small spheres in cells closer to the outer sample surface (top of picture) and it becomes thinner and smoother towards the interior of the sample. The uneven thickness of the deposit is most likely due to partial solution bypassing between the PHIPE and the glass walls of the tubular cell used. Nevertheless, there were no uncoated cells left in the interior of the sample, in contrast to previous attempts from stationary solutions [20]. The electroactive surface area of the Ni/PHIPE composite was determined as before by the amount of Ni hydroxide formed and reduced during cyclic voltammetry in 0.5 M NaOH. Figure 10(A) shows the cyclic voltammogram at 10 mV s^{-1} of a Ni/PHIPE composite electrode in 0.5 M NaOH whereas Figure 10(B) shows a similar voltammogram recorded at a polished Ni disc electrode, in the potential region in which a monolayer of α-$Ni(OH)_2$ is formed/stripped [30, 31]. In the latter, the peaks corresponding to the oxidation of Ni to α-$Ni(OH)_2$ (anodic peak at about −0.7 V vs SCE) and the reduction of the latter upon potential reversal (cathodic peak at about −1.1 V vs SCE), are similar to those reported [30, 31]. In the case of the Ni/PHIPE electrode the voltammetry is less defined since it is affected by higher charging currents ([43, 44]) and, more important, since electroless nickel produced from hypophosphite baths is a Ni–P alloy having different catalytic properties than bulk Ni. The charge associated with the formation/reduction of a monolayer of α-$Ni(OH)_2$ is 514 μC cm^{-2} [30, 31] and estimation of the area under the anodic peak gives an electroactive

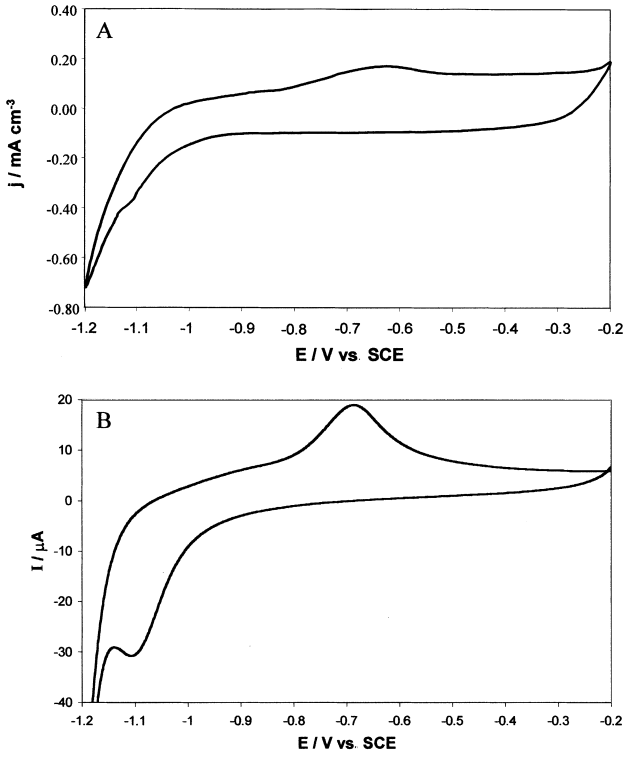

Fig. 10. (A) Voltammogram recorded in a deaerated 0.5 M NaOH solution at a Ni/PHIPE composite produced by electroless plating through the polymer, at a potential scan rate of 10 mV s^{-1}; (B) Same as before but for a smooth Ni disc electrode.

surface area which translates to a specific surface area of 1800 m^2 m^{-3}, which is comparable with the lower values, reported for some Cu, RVC and Ni foam materials [38].

4. Conclusions

A recently tested [20–22] polymer template electrodeposition route for porous Ni electrode coatings production was further developed. Uniform and adherent porous deposits were obtained on larger electrode substrates by flowing the electroplating solution through a block of a generic polymer (PHIPE) fitted in the interelectrode gap of a flow-by parallel plate electrochemical cell. The morphology and quality of the deposit was influenced by the local current density within the polymer cells and was also dependant on current density and the thickness of the polymer interelectrode layer. As the latter increases so do the ohmic losses and a detrimental effect on the uniform development of the three-dimensional deposit is observed. The use of thinner polymer layers would be impractical due to very high-pressure drops encountered and, instead, substrate embedment in the polymer block at locations close to the block surface could be an alternative in reducing ohmic losses. Nevertheless, for current densities of the order of 5 mA cm^{-2}, an interelectrode gap of 15 mm and a solution flow velocity of 1.5 cm s^{-1}, adherent deposits made of large aggregates of 5–20 μm, separated by similar size voids and consisting of smaller nodules, were deposited across the entire electrode surface. They showed comparable current densities for hydrogen evolution to that of typical sintered Ni electrodes of similar thickness and, although they are characterized by lower porosity and electroactive surface areas, the utilization of the latter for hydrogen evolution is higher, possibly due to the absence of pore clogging by hydrogen gas.

Finally, Ni/PHIPE composites were produced by internally coating the porous polymer with electroless plated Ni from a flowing solution. The resulting material had a specific electroactive surface area comparable with that of low pore per inch grades of reticulated metal foams and, if optimised, could find applications as a three dimensional electrode, a porous lightweight support for active mass incorporation of Ni–Cd batteries [13, 35] or as a metallized membrane material.

Acknowledgements

The authors wish to thank EPSRC (UK) for a studentship to I.J.B. S.S. acknowledges an ΕΠΕΤ program research grant from the General Secretariat of Research and Technology (Greece) and a NATO SFP grant (Preparatory Grant SfP 977986).

References

1. Y.M. Sun and S.J. Khang, *Ind. Eng. Chem. Res.* **29** (1990) 231.
2. K. Li and N. Li, *Sep. Sci. Tech.* **28** (1993) 1085.
3. R.J. Wakeman and M.N. Sabri, *Chem. Eng. Res. Design* **73** (1995) 455.
4. S. Ye, A.K. Vijh and L.H. Dao, *J. Electrochem. Soc.* **143** (1996) L7; **144** (1997) 90.
5. A. Czerwiński, M. Dmochowska, M. Grdeń, M. Kopczyk, G. Wójcik, G. Mlynarek, J. Kolata and J.M. Skowroński, *J. Power Sources* **77** (1999) 28.
6. O. Chyan, J.-J. Chen, M. Liu, M.G. Richmond and K. Yang, *Mat. Res. Soc. Symp. Proc.* **393** (1995) 265.
7. W. Bacher, K. Bade, K. Leyendecker, W. Menz, W. Stark and A. Thommes, *in* N. Masuko, T. Osaka and Y. Ito (Eds) 'Electrochemical Technology' (Kodansha Ltd, Tokyo, 1996).
8. I.F. Cheng and C.R. Martin, *Anal. Chem.* **60** (1988) 2163.
9. J.C. Hulteen and C.R. Martin, *J. Mater. Chem.* **7**(7) (1997) 1075.
10. T.M. Whitney, J.S. Jiang, P.C. Searson and C.L. Chien, *Science* **261** (1993) 1316.
11. H.B. Suffredini, J.L. Cerne, F.C. Crnkovic, S.A.S. Machado and L.A. Avaca, *Int. J. Hydrogen Energy* **25** (2000) 415.
12. O. Bohme, F.U. Leidich, H.J. Salge and H. Wendt, *Int. J. Hydrogen Energy* **19** (1994) 349.
13. K. Wall, 'Modern Chlor-Alkali Technology', Vol. 3 (Ellis Horwood, Chichester, UK, 1986).
14. C.A. Vincent and B. Scrosati, 'Modern Batteries', 2nd Edn (Arnold, London, 1997).
15. T.C. Benjamin, E.H. Camera and L.G. Marianowski, *in* 'Handbook of Fuel Cells' (Institute of Gas Technology, Chicago, 1980).
16. V. Anantharaman and P.N. Pintauro, *J. Electrochem. Soc.* **141**(10) (1994) 2729.

17. D.A. Cox, PhD thesis, Southampton, UK (1981).
18. C.J. Brown, D. Pletcher, F.C. Walsh, J.K. Hammond and D. Robinson, *J. Appl. Electrochem.* **24**(2) (1994) 95.
19. S. Rausch and H. Wendt, *J. Electrochem. Soc.* **143**(9) (1996) 2852.
20. S. Sotiropoulos, I.J. Brown, G. Akay and E. Lester, *Mater. Lett.* **35** (1998) 383.
21. I.J. Brown, D. Clift and S. Sotiropoulos, *Mater. Res. Bull.* **34**(7) (1999) 1055.
22. I.J. Brown and S. Sotiropoulos, *J. Appl. Electrochem.* **30** (2000) 107.
23. D. Barby and Z. Haq, *European Patent 0 060 138* assigned to Unilever (1982).
24. J. Williams, *Langmuir* **4** (1988) 44.
25. N.R. Cameron and D.C. Sherrington, *Adv. Polymer Sci.* **126** (1996) 163.
26. F.A. Lowenheim, *in* 'Electroplating' (McGraw-Hill, New York 1978).
27. A.K. Graham, 'Electroplating Engineering Handbook' (Van Nostrand, New York, 1971).
28. R. Winand, *Electrochim. Acta* **39**(8/9) (1994) 1091.
29. L. Cai and H.Y. Cheh, Meeting Abstracts of the 191st Meeting of The Electrochemical Society, Abstract 51, Montreal (1997), p. 58.
30. F. Hahn, B. Beden, M.J. Croissant and C. Lamy, *Electrochim. Acta* **31**(3) (1986) 335.
31. S.A.S. Machado and L.A. Avaca, *Electrochim. Acta* **39**(10) (1994) 1385.
32. D.A. Cowan and J.H. Brown, *Ind. & Eng. Chem.* **51** (1959) 1445.
33. C. Ponce-de-Leon and R.W. Field, *J. Appl. Electrochem.* **30**(9) (2000) 1087–1090.
34. C.J. Brown, D. Pletcher, F.C. Walsh, J.K. Hammond and D. Robinson, *J. Appl. Electrochem.* **23** (1993) 38.
35. D. Pletcher and F.C. Walsh, 'Industrial Electrochemistry', 2nd edn (Blackie Academic and Professional, London, 1993).
36. D.J. Pickett and K.L. Ong, *Electrochim. Acta* **19** (1974) 785.
37. D.J. Pickett, 'Electrochemical Reactor Design', 2nd edn (Elsevier, Amsterdam, 1979).
38. S. Langlois and F. Coeuret, *J. Appl. Electrochem.* **19** (1989) 51.
39. A. Montillet, J. Comiti and J. Legrand, *J. Appl. Electrochem.* **24** (1994) 384.
40. A. Montillet, J. Comiti and J. Legrand, *J. Mater. Sci.* **27** (1992) 4464.
41. J.M. Coulson, J.F. Richardson, J.R. Backhurst and J.H. Harker, 'Chemical Engineering', 4th edn, Vol. 2 (Pergamon Press, Oxford, 1991).
42. R.E. Meredith and C.W. Tobias, 'Advances in Electrochemistry and Electrochemical Engineering', Vol. 2 (Wiley Interscience, London, 1965). pp. 15–47.
43. A.N. Correia and S.A.S. Machado, *Electrochim. Acta* **43** (3–4) (1998) 367.
44. M.J. De Giz, S.A.S. Machado, L.A. Avaca and E.R. Conzalez, *J. Appl. Electrochem.* **22** (1992) 973.